Origin of Roll Waves in Horizontal Gas-Liquid Flows

The mechanism of formation of roll waves on a horizontal liquid layer sheared by a gas flow is examined. Measurements of the wave amplitude spectrum show that, for liquid film Reynolds numbers greater than about 100, roll waves evolve from disturbances that initially have wavelengths much longer than the film thickness and which grow slowly with distance. Predictions of linear stability analysis are shown to agree well with the observation of these instabilities and not the visual transition to roll waves as was suggested in earlier studies. For very thin films, the data do not give conclusive proof of the origin of roll waves, but it is speculated that these are actually solitary waves which have begun to break.

Kenneth Bruno and M. J. McCready
Department of Chemical Engineering
University of Notre Dame
Notre Dame, IN 46556

Introduction

The wave structure in gas-liquid flows exerts influence on the pressure drop and transport rates, determines atomization, and under certain conditions may signal impending changes in flow regime. The dominant wave type under a wide range of conditions in both stratified and annular flows are roll or disturbance waves which have been described by Hanratty and Engen (1957). These waves generally have wavelengths much larger than the film thickness and are observed visually to be breaking waves which travel through the flow system without dying out. Roll waves are of interest in the determination of the character of two-phase flows because they carry and mix fluid (Dukler, 1977), cause very strong fluctuations in the wall shear stress, may be of importance in the formation of slugs (Kordyban, 1985), and appear to be associated with atomization (Woodmansee and Hanratty, 1969, Hanratty and Hershman, 1961; Miya et al., 1971).

In vertical flows, studies of the interfacial wave behavior have been done by Telles and Dukler (1970), Chu and Dukler (1974, 1975), Webb and Hewitt (1975), Nencini and Andreussi (1982), and Martin and Azzopardi (1985). Telles and Dukler (1970) note that two types of waves are observed on vertical films, long wavelength dominant waves which carry fluid (which are very similar to the roll waves of the horizontal case), and smaller waves which exist on the substrate.

Roll waves in horizontal flows have been examined by Hanratty and Hershman (1961), Miya et al. (1971), and Andreussi et al. (1985). A wide range of viscosities have been covered and the regions of existence have been identified by visual observations. These researchers have used linear stability theory to predict the onset of roll waves. The basic premise behind their theoretical predictions is that the roll waves are formed from an instability which causes waves much longer than the film thickness to become unstable. Short wavelength waves, which are already present, influence this growth only through their effect on the surface roughness. For films where the liquid Reynolds number is greater than about 200, the prediction of linear theory done by Hanratty and Hershman (1961) provides good quantitative agreement. However, a direct link between the initial instability, which causes these waves and their visual occurrence, has not been established.

For thinner films, the linear stability theory presented by Hanratty and Hershman (1961) predicts waves will occur when none are observed. Andreussi et al. (1985) used an approach which included a more detailed description of the turbulent gas flow. They found that, if the interfacial shear stress variation caused by the gas flow does not immediately follow the surface variation but is out of phase by approximately the wavelength of a typical simultaneously occurring capillary wave, then long wavelength disturbances are expected to be stable. The transition to roll waves is predicted when the stress variation shifts back in-phase with the shape of the long wave because of a sudden increase in the surface roughness. Experiments with fluids of increasing viscosity provide some support for this approach. It is, however, difficult to believe that a relaxation effect could cause the stress variation to be as much as a whole wavelength out of phase. In addition, there is no inherent reason to expect that linear theories could always predict the origin of such highly nonlinear disturbances.

In this paper the origin of roll waves in gas-liquid flows is

reexamined. Quantitative measurements of the surface, which provide wave spectra and surface tracings, are used to demonstrate the type of disturbances from which roll waves occur. For relatively thick films, two distinct peaks are observed in the spectrum corresponding to the expected two different mechanisms of wave formation. Waves associated with the lower frequency peak appear to be precursors of roll waves; however, since they exist under conditions where roll waves do not, either nonlinear effects stabilize these waves or a greater flow direction length is needed for roll wave formation. For thinner films, only a single wave peak is observed suggesting that roll waves may evolve by a different process.

Theoretical Background

As shown by Craik (1966) and Hanratty (1983), two different wave types caused by two distinct mechanisms can be formed on liquid films as the result of the action of a gas flow. Waves with wavelengths much shorter than the film thickness form as the result of irreversible energy transfer from the gas, primarily due to the pressure component in-phase with the wave slope (sheltering) (Jeffreys, 1925), exceeding the rate of viscous dissipation. A reversible process, the inertial forces caused by the flow and pressure variations in phase with the wave height (Bernoulli type) overcoming the restoring forces of gravity and surface tension, is responsible for formation of waves much longer than film thickness. However, as will be shown below, waves observed experimentally may have certain features of both of these wave types.

To predict the stability of the short wavelength waves, the Orr-Sommerfeld analysis, described by Cohen and Hanratty (1965) and Hanratty (1983) will be used. Our present interest is to compare their predictions of unstable wavelengths with our measurements. It will be shown that this instability corresponds to the higher frequency peak in our spectral measurements.

To determine regions of instability for long wavelength waves, the integral boundary-layer approach used by Hanratty (1983) and Andreussi et al. (1985) will be used with improved values for the various flow parameters. From a solution to the complete Eigenvalue problem, we find that neutral stability criteria are best described as occurring over a range of gas Reynolds numbers (within the accuracy of the values for the various flow variables), and that long wavelength waves are predicted to be unstable in regions where our experiments show their existence and no roll waves are observed. It should be noted that any linear stability analysis will be valid only for determining the initial growth rates and speeds and cannot predict the eventual fate of waves.

Long wavelength stability analysis

The system configuration, a horizontal, cocurrent flow, is shown in Figure 1. A turbulent gas flow is shearing a liquid layer such that the liquid flow becomes unstable. Roll waves are assumed to grow out of disturbances which are much longer than the film thickness. This allows the governing Navier-Stokes equations to be simplified using boundary-layer approximations. Integration of the liquid-phase continuity and x-momentum equations under these assumptions yields (Hanratty, 1983),

$$h\frac{\partial u_a}{\partial x} + u_a\frac{\partial h}{\partial x} + \frac{\partial h}{\partial t} = 0 \tag{1}$$

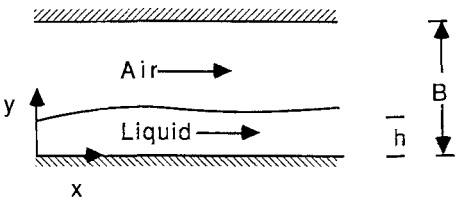

Figure 1. Horizontal gas-liquid flow system.

and

$$\frac{\partial u_a}{\partial t} + (2\Gamma - 1)u_a\frac{\partial u_a}{\partial x} + (\Gamma - 1)\frac{u_a^2}{h}\frac{\partial h}{\partial x} + u_a^2\frac{\partial \Gamma}{\partial x} = \frac{\tau_s}{\rho_L h} - \frac{\tau_w}{\rho_L h} - \frac{1}{\rho_L}\frac{\partial P_s}{\partial x} - g\frac{\partial h}{\partial x} + \sigma\frac{\partial^3 h}{\partial x^3}. \tag{2}$$

In these equations, the pressure in the liquid is given by

$$p = P_s + \rho_L g(h - y) - \sigma\frac{\partial^2 h}{\partial x^2} \tag{3}$$

and the average x velocity, u_a, is defined as

$$u_a h = \int_0^h u\, dy. \tag{4}$$

A velocity profile shape factor, Γ (Hanratty and Hershman, 1961) is introduced,

$$\Gamma h u_a^2 = \int_0^h u^2\, dy \tag{5}$$

which typically varies between 1.2–1.6.

Similarly, upon integration the resulting gas-phase equations of continuity and motion are:

$$-\frac{\partial h}{\partial t} + \frac{\partial}{\partial x}[(B - h)U_a] = 0 \tag{6}$$

$$\frac{\partial}{\partial t}[(B - h)U_a] + \frac{\partial}{\partial x}[(B - h)U_a^2] = -\left(\frac{B - h}{\rho_G}\right)\frac{\partial P_s}{\partial x} - \frac{\tau_s - \tau_B}{\rho_G}. \tag{7}$$

Gas Reynolds numbers are sufficiently large to assume a flat velocity profile resulting in $\Gamma_G = 1$.

To identify conditions where waves occur, it is necessary to determine the stability of Eqs. 1, 2, 6 and 7 to small amplitude disturbances. Waves generated by the gas flow are observed to be initially periodic so that a sinusoidal disturbance of the form

$$h' = a\exp i\alpha(x - ct) \tag{8a}$$

where

$$h = \bar{h} + h' \tag{8b}$$

is appropriate. The fluctuation h' is the deviation of the instantaneous film height from the average film height. Disturbances of

the velocity and stress fields are represented by

$$u_a = \bar{u}_a + u'_a \tag{8c}$$

$$U_a = \bar{U}_a + U'_a \tag{8d}$$

$$\tau_s = \bar{\tau}_s + \tau'_s \tag{8e}$$

$$\tau_w = \bar{\tau}_w + \tau'_w \tag{8f}$$

$$P_s = \bar{P}_s + P'_s. \tag{8g}$$

An overbar indicates a time-averaged quantity, and the primed quantities are wave-induced fluctuations. Due to the small amplitude of the imposed disturbance, h', the resulting fluctuating components are also linear responses designated by

$$\frac{u'_a}{\hat{u}_a(y)} = \frac{U'_a}{\hat{U}_a(y)} = \frac{\tau'_s}{\hat{\tau}_s} = \frac{\tau'_w}{\hat{\tau}_w} = \frac{P'_s}{\hat{P}_s} = a \exp i\alpha(x - ct) \tag{8h}$$

where a caret denotes a complex quantity. Using the observation that the viscosities and densities of air and the various liquids differ greatly and that waves form on the liquid as a result of force and energy provided by the gas flow while the effect of the liquid on the gas is only through an average stress, equations for the two phases can be solved separately. As a consequence, Eqs. 1, 2 and 8 constitute an Eigenvalue problem where the wave speed c is the complex Eigenvalue. The real part yields the wave speed and for positive values of the imaginary part of c, the wave is unstable to growth.

The substitution of Eqs. 8 into Eqs. 1 and 2 and linearization with respect to wave amplitude a results in the governing liquid phase stability equations for long wavelength waves. Continuity reduces to

$$\bar{h}\hat{u}_a = c - \bar{u}_a. \tag{9}$$

The linearized x-momentum stability equation becomes

$$c^2 + \bar{u}_a^2\bar{\Gamma} - 2\bar{u}_a\bar{\Gamma}c - \bar{h}\bar{u}_a^2\hat{\Gamma} = \frac{i\hat{\tau}_s}{\rho_L\alpha} - \frac{i\hat{\tau}_w}{\rho_L\alpha} - \frac{i}{\rho_L}\frac{d\bar{P}_s}{dx} + \frac{\bar{h}\hat{P}_s}{\rho_L} + g\bar{h} + \frac{\alpha^2\sigma\bar{h}}{\rho_L} \tag{10}$$

where Eq. 9 has been used to eliminate $\bar{u}_a$. Equation 10 is solved to determine the stability of long wavelength waves for small αh under given flow conditions. However, to solve Eq. 10, expressions for $\bar{\Gamma}$, $\hat{\Gamma}$, $\hat{\tau}_s$, $\hat{\tau}_w$ and $\hat{P}_s$ are required.

Evaluation of Γ. Calculation of the velocity profile shape factor Γ requires knowledge of the velocity profile in the liquid phase. Following a procedure similar to Pai (1953), a semiempirical estimation of this turbulent velocity profile can be derived. Assuming fully developed flow and that the turbulent fluctuations are only a function of y, the x component of momentum reduces to

$$0 = -\frac{\partial\bar{p}}{\partial x} + \frac{d}{dy}\left(\mu\frac{d\bar{u}}{dy} - \rho_L\overline{u'v'}\right). \tag{11}$$

The y component of motion is

$$0 = -\frac{\partial\bar{p}}{\partial y} - \rho_L\frac{d}{dy}(\overline{v'^2}) \tag{12}$$

from which it is deduced that $(\partial\bar{p})/(\partial x)$ cannot be a function of y, hence allowing separation and integration of Eq. 11. Integrating Eq. 11 twice and applying the boundary conditions

$$\bar{u}(0) = 0 \tag{13a}$$

$$\bar{\tau}(0) = \bar{\tau}_w \tag{13b}$$

yields

$$\bar{u} = \int_{y=0}^{y}\frac{\rho_L\overline{u'v'}}{\mu}dy + \frac{\bar{\tau}_s - \bar{\tau}_w}{2\mu\bar{h}}y^2 + \frac{\bar{\tau}_w}{\mu}y \tag{14}$$

where

$$\frac{\partial\bar{p}}{\partial x} = \frac{\bar{\tau}_s - \bar{\tau}_w}{\bar{h}}. \tag{15}$$

To avoid having to evaluate the integral of the Reynolds stress, a velocity profile for the liquid is needed which contains a term that accounts for turbulent effects. It will be assumed that a polynomial profile, which allows for a correction term added to the laminar solution, will be adequate. Under this assumption, the turbulent time-averaged velocity profile can be written as

$$\bar{u} = D_T + A_Ty + B_Ty^2 + C_Ty^n. \tag{16}$$

The constant C_T accounts for the turbulent character of the velocity profile; for C_T equal to zero, a laminar profile is obtained. Application of boundary condition 13a shows $D_T = 0$. The remaining three constants are determined by solving Eqs. 14 and 16 simultaneously and applying the boundary conditions

$$\bar{u}(\bar{h}) = u_s \tag{17a}$$

$$\overline{u'v'}(0) = 0 \tag{17b}$$

$$\overline{u'v'}(\bar{h}) = 0. \tag{17c}$$

The resulting values of A_T, B_T and C_T are

$$A_T = \frac{\bar{\tau}_w}{\mu} \tag{18}$$

$$C_T = \frac{u_s - \frac{\bar{\tau}_w - \bar{\tau}_s}{2\mu}\bar{h}}{\bar{h}^n\left(1 - \frac{n}{2}\right)} \tag{19}$$

$$B_T = \frac{\bar{\tau}_s - \bar{\tau}_w - \mu nC_T\bar{h}^{n-1}}{2\mu\bar{h}}. \tag{20}$$

Using experimental data for all the parameters at several liquid and gas Reynolds numbers, the value of the exponent n was varied until the resulting average velocity calculated from the insertion of Eq. 16 into Eq. 4 equalled the average velocity calculated from the liquid Reynolds number. A value of $n = 1.2$ gave the best agreement with data.

As with the other quantities, $\bar{\Gamma}$ may be written as the sum of fluctuating and average quantities. Use of Eqs. 5, 8 and 16 yields

$$\bar{\Gamma} = \frac{1}{\bar{u}_a^2}\left[\frac{A_T^2\bar{h}^2}{3} + \frac{B_T^2\bar{h}^4}{5} + \frac{C_T^2\bar{h}^{2.4}}{3.4} + \frac{A_TB_T\bar{h}^3}{2} + \frac{2A_TC_T\bar{h}^{2.2}}{3.2} + \frac{2B_TC_T\bar{h}^{3.2}}{4.2}\right]. \quad (21)$$

Note that to derive Eq. 21, $\bar{u}$ in Eq. 5 has been set equal to the turbulent time-averaged profile u from Eq. 16.

Hanratty (1983) defines $\hat{\Gamma}$ as

$$\hat{\Gamma} = \frac{d\bar{\Gamma}}{dR_L} R_L \frac{c}{\bar{u}_a\bar{h}}. \quad (22)$$

Equation 21 was utilized to calculate $\bar{\Gamma}$ for liquid Reynolds numbers between 200 and 2,000. An examination of our calculated values for $\bar{\Gamma}$ indicated that it was a weak function of R_L. To determine the derivative, $(d\bar{\Gamma})/(dR_L)$, a plot of $\bar{\Gamma}$ vs. R_L at constant gas Reynolds number was constructed. Figure 2 shows this plot which has an average slope of -0.0001.

Andreussi et al. (1985) calculate $\bar{\Gamma}$ from

$$\bar{\Gamma} = \frac{h^+}{R_L^2}\int_0^{h^+} u^{+2}(y^+)\, dy^+ \quad (23)$$

where the "+" variables are made dimensionless with v^* and ν; u^+ is calculated from the van Driest mixing length equation. Andreussi assumed the integrand to be independent of R_L implying that the dimensionless profiles are self-similar. To test this hypothesis, Eq. 21 was likewise cast in dimensionless "plus" quantities and the resulting profiles were found to be not self-similar. It is believed that the waves introduce additional length scales which are not easily incorporated in the analysis. For this reason, $(d\bar{\Gamma})/dR_L)$ cannot be accurately determined from Eq. 23.

Evaluation of $\hat{P}_s$. The defining equation for $\hat{P}_s$ (Hanratty, 1983) is obtained by solving the gas-phase equations of continuity (Eq. 6) and motion (Eq. 7), and by again utilizing Eqs. 8a–h. Keeping only terms of first order in amplitude gives

$$\hat{P}_s = \frac{i(\hat{\tau}_s - \hat{\tau}_B)}{\alpha(B - \bar{h})} - \frac{\rho_G(\bar{u}_a - c)^2}{B - \bar{h}} - \frac{i\partial\bar{P}_s}{\alpha\partial x}\frac{1}{(B - \bar{h})}. \quad (24)$$

Equation 24 is valid in the long wavelength limit. It is, however, interesting to note that calculations of $\hat{P}_s$ by Abrams (1984) using a turbulence model and the assumption of short wavelength (no interference by the top wall) yield very similar numerical values for the range of interest in this study.

Evaluation of the Shear Stress Fluctuations. Hanratty (1983) derived an expression for the interfacial wave-induced shear stress variation amplitudes for a roughened surface which separates into

$$\hat{\tau}_{sR} = \bar{\tau}_s\left(\frac{2}{B} + \frac{R_L}{f_s}\frac{\partial f_s}{\partial R_L}\frac{c_R}{\bar{u}_a}\frac{1}{\bar{h}}\right) \quad (25a)$$

and

$$\hat{\tau}_{sI} = 0. \quad (25b)$$

Andreussi et al. (1985) present friction factor–R_L data and provide the relationship

$$\frac{R_L}{f_s}\frac{\partial f_s}{\partial R_L} = \frac{\bar{u}_a}{u_s}\left(\frac{0.023h_g^+}{0.4793 + 0.023h_g^+}\right) \quad (26)$$

which is substituted into Eq. 25a. The Henstock and Hanratty (1976) correlation can be employed to calculate $h_g^+(R_L)$.

The bottom wall shear variation amplitude $\hat{\tau}_w$ is shown by Hanratty (1983) to be

$$\hat{\tau}_w = \frac{3\mu\bar{u}_aA(R_L)}{\bar{h}^2}\left[\frac{c}{\bar{u}_a} - 2 + \frac{c}{\bar{u}_a}\frac{R_L}{A(R_L)}\frac{dA(R_L)}{dR_L}\right] \quad (27)$$

with the function $A(R_L)$ included to account for turbulence effects.

The upper wall shear stress variation amplitude, $\hat{\tau}_B$, is given by Hanratty (1983) as

$$\hat{\tau}_{BR} = \frac{2\bar{\tau}_B}{B} \quad (28a)$$

and

$$\hat{\tau}_{BI} = 0. \quad (28b)$$

Linear Stability Solution. Equation 10 governs the long wavelength stability problem. Utilizing the above expressions for the magnitudes of the fluctuating quantities, a complex root finder was employed to solve Eq. 10 for c when R_L was greater than 200. This procedure was found to be much easier than the one used by Andreussi et al. (1985) which was to set c_i equal to zero and then adjust flow parameters to satisfy the equations. The results are presented below.

Considerable insight concerning the effect of various terms on long wavelength wave instabilities may be gained by separating

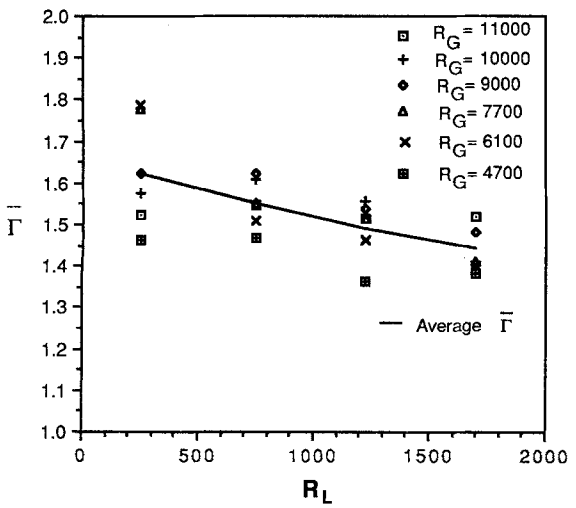

Figure 2. Plot of $\bar{\Gamma}$ calculated from experimental data using Eq. 21.

Eq. 10 into its real and imaginary components:

$$-c_I^2 + c_R^2 - 2\bar{\Gamma}\bar{u}_a c_R + \bar{\Gamma}\bar{u}_a^2 - \bar{h}\bar{u}_a^2\hat{\Gamma}_R = -\frac{\hat{\tau}_{sI}}{\rho_L\alpha} + \frac{\hat{\tau}_{wI}}{\rho_L\alpha} + \frac{\alpha\bar{h}\hat{P}_{sR}}{\rho_L\alpha} + g\bar{h} + \frac{\alpha^2\sigma\bar{h}}{\rho_L} \quad (29)$$

$$-\bar{h}u_a^2\hat{\Gamma}_I + 2c_I(c_R - \bar{\Gamma}\bar{u}_a) = \frac{\hat{\tau}_{sR}}{\rho_L\alpha} - \frac{\hat{\tau}_{wR}}{\rho_L\alpha} + \frac{\alpha\bar{h}\hat{P}_{sI}}{\rho_L\alpha} - \frac{1}{\alpha\rho_L}\frac{d\bar{P}_s}{dx}. \quad (30)$$

By comparing solutions of Eq. 10 with Eqs. 29 and 30 for c_R and c_I when αh is between approximately 0.2 and 0.005, it can be seen that Eq. 29 controls the wave speed and Eq. 30 primarily determines the wave growth. Closer examination of Eq. 30 shows that $\hat{\tau}_{sR}$ and $\hat{P}_{sI}$ are destabilizing.

However, for αh less than approximately 0.005, the extremely long wavelength limit, the situation reverses and Eq. 30 defines the wave speed. The growth rate is provided by Eq. 29 where inertial and $\hat{P}_{sR}$ terms are the dominant destabilizing terms with gravity acting as the primary stabilizing force.

Short wavelength stability analysis

An Orr-Sommerfeld analysis of the gas-liquid flow under the assumption of high gas and liquid Reynolds numbers and short wavelengths has been shown by Hanratty (1983) to yield the following secular equation for the Eigenvalue c,

$$\alpha(u_s - c)^2\coth(\alpha\bar{h}) - \left(\frac{d\bar{u}}{dy}\right)_s(u_s - c) = G + \frac{i\hat{\tau}_s}{\rho_L}\left[\coth(\alpha\bar{h}) - \frac{1}{\alpha(u_s - c)}\left(\frac{d\bar{u}}{dy}\right)_s\right] - (\alpha\bar{h})^{1/2}\left(-i\frac{\bar{h}c}{\nu_L}\right)^{-1/2}[\alpha(u_s - c)^2 (1 - \coth^2(\alpha\bar{h}))] + 4i(\alpha\bar{h})\left(\frac{\bar{h}(u_s - c)}{\nu_L}\right)^{-1} \alpha(u_s - c)^2\left[\coth(\alpha\bar{h}) - \frac{1}{\alpha(u_s - c)}\left(\frac{d\bar{u}}{dy}\right)_s\right] \quad (31)$$

where

$$G = \frac{\hat{P}_s}{\rho_L} + \frac{\sigma\alpha^2}{\rho_L} + g. \quad (32)$$

Because these waves are expected to have wavelengths much less than the depth of the gas phase, calculations for turbulent flow over short wavelength waves done by Abrams (1984) will be used to evaluate the wave-induced fluctuations in the pressure and stress.

Experiment

Description of flow system

The gas-liquid flows were studied in a horizontal, rectangular channel which has a flow area 2.54 cm high, 30.5 cm wide, and a total length of about 8.5 m. The flow configuration is essentially the same as was used by Andreussi et al. (1985). Air is pumped by a centrifugal blower through a converging entrance section into the end of the channel and liquid enters through the channel bottom at the same end. Both the air and liquids are filtered to prevent contamination by solid particles which may cause surface films. An oscillating paddle is located at the front of the channel. It consists of a brass plate extending across the width of the channel and when not in operation, is flush with the bottom wall. Both the amplitude and the frequency of the paddle are adjustable, allowing the introduction of artificial waves of various sizes and frequencies into the system.

Wave probes

Wave properties were determined by using parallel wire conductance probes which have been described in great detail previously by Miya et al. (1971) and McCready (1986). Wire diameters of 0.000127 m with spacings of about 0.002 m were used. A 30-kHz-sine wave was applied to one wire and the resulting voltage drop converted to a variable voltage signal proportional to film height using an electrical circuit described in a thesis by Lin (1985). The liquid conductance was adjusted to a value in the range of 200 μmho so that a linear relation between film height and voltage was obtained. The probes were calibrated using a contact probe technique which has been described by Henstock (1977). The analog voltage signal from the film height analyzer is sampled using a PDP 11/24 microcomputer and stored for later analysis. Data are presented here both in the form of surface tracings and frequency spectra. The spectral function $\phi(f)$ is defined as

$$\overline{a^2} = \int_0^\infty \phi(f)\, df \quad (33)$$

where $\overline{a^2}$ is the variance of the instantaneous surface displacement.

Interfacial stress

The pressure drop at each set of flow conditions was measured using a micromanometer. The gas-phase velocity profile and the location of the maximum velocity were determined by traversing a Pitot tube between the gas-liquid interface and the top of the channel. The maximum velocity is displaced slightly above the gas-phase centerline due to the interfacial roughness. The zero stress lies below the maximum velocity plane (Miya, 1968). Interfacial and wall shear stresses may be calculated from the pressure drop, average film height and location of the zero stress plane as the stress must vary linearly with distance. However, the uncertainty of the exact zero stress location introduces a potential error of approximately 10% of the stress values.

Interfacial velocities

Interfacial velocities were determined by placing thin computer card punched rectangles onto the gas-liquid interface and timing their progression over a known distance. Reproductibility was within 5%. There was no visual interference of the waves with the squares or vice versa as the waves traveled through the squares and did not alter their form. Visual observations revealed that the depth of the squares was nearly equally distributed in the liquid and gas phases and therefore it is believed that an accurate measurement of the interfacial velocity was obtained.

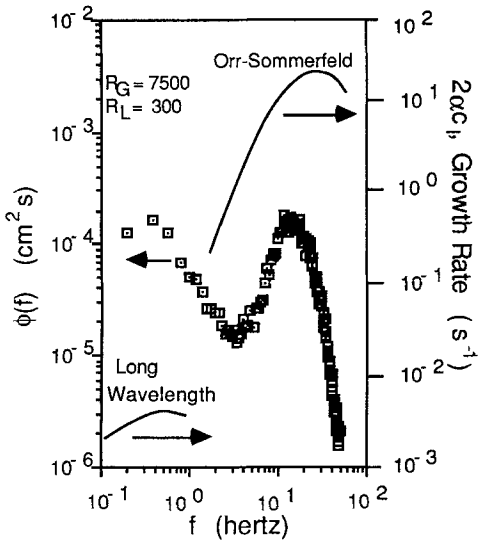

Figure 3. Measured wave spectrum showing 2 peaks and growth rates predicted by linear stability theory for both wave types.

Results

Figure 3 shows the wave amplitude spectrum, $\phi(f)$, measured for liquid and gas Reynolds numbers of 300 and 7,500, respectively. The liquid is a water-glycerin solution with a viscosity of 5×10^{-3} N · s/m^2. (We note that additional experiments with mixtures of higher and lower viscosities gave essentially the same roll wave transition and qualitative wave behavior for the high liquid Reynolds number region and will not be presented.) Two distinct peaks are seen at about 0.3 Hz and 10 to 20 Hz corresponding to waves with long and short wavelengths. In Figure 4, a surface tracing shows the interface as measured by the wave probe. Also shown in figure 4 are digitally filtered versions of the same surface tracing which clearly display the presence of short and long wavelength waves.

Calculations for growth rates as a function of frequency for long wavelength, Eq. 10 and Orr-Sommerfeld, Eq. 31, stability analyses described above are also shown on Figure 3. The stability analyses predict that waves should occur in two distinct frequency ranges, less than 1 Hz and 10–40 Hz. An important feature of the predictions is the relative growth rates of the two ranges. High-frequency waves have maximum rates which are 3–4 orders of magnitude higher than long wavelength waves. This suggests that the short-wavelength waves will form much more rapidly than longer wavelength disturbances which may take several seconds to reach measurable amplitudes. The predictions of the fastest growing waves are in good qualitative agreement with the location of the peaks in the measured wave spectrum. In addition, short waves are visible almost immediately at the inlet of the channel while longer wavelength waves (as will be seen below) grow slowly with distance supporting the qualitative prediction of much slower growth for long wave disturbances.

More extensive predictions of growth rates as a function of gas velocity for R_L = 740 are shown in Figure 5. As expected, growth rates for both wave types increase with R_G and short-wavelength waves are seen to grow at a much faster rate than low frequency waves. It is interesting to compare the magnitudes of the predicted growth rates in Figures 3 and 5. For the Orr-Sommerfeld analysis, little effect of the change in R_L occurs consistent with the short-wavelength approximation. However, for the long-wavelength case, the growth rate increases by about 1 order of magnitude exhibiting the strong role that film depth plays when its value is much less than the wavelength.

The measured spectrum as a function of gas velocity is shown in Figure 6. Both peaks are seen to increase with gas Reynolds number. The observed transition to roll waves, which occurs at about R_G = 11,000 agreeing exactly with Andreussi et al. (1985), is not associated with any qualitative change in the spectrum only further increases in the low frequency peak. It is important to note that low-frequency waves, which are apparently the precursors to roll waves, are present at gas velocities much lower than the visual transition.

The spectrum evolution as a function of fetch (distance from initial gas-liquid contact point) for conditions where no roll waves are observed is shown in Figure 7. It is seen that, as predicted by stability theory, the low frequency peak grows continually with distance; a smaller increase in the short-wavelength

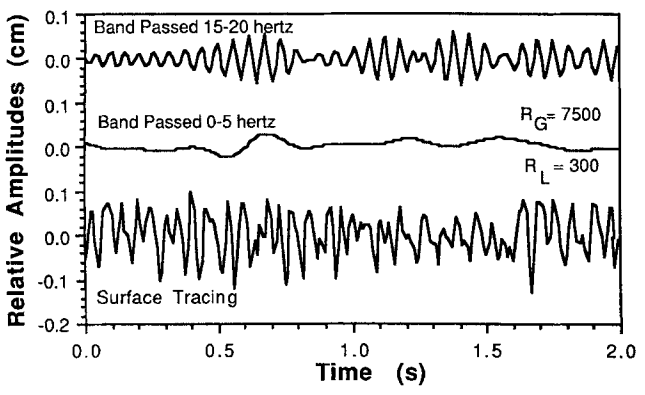

Figure 4. Surface tracings showing the original and filtered signals.

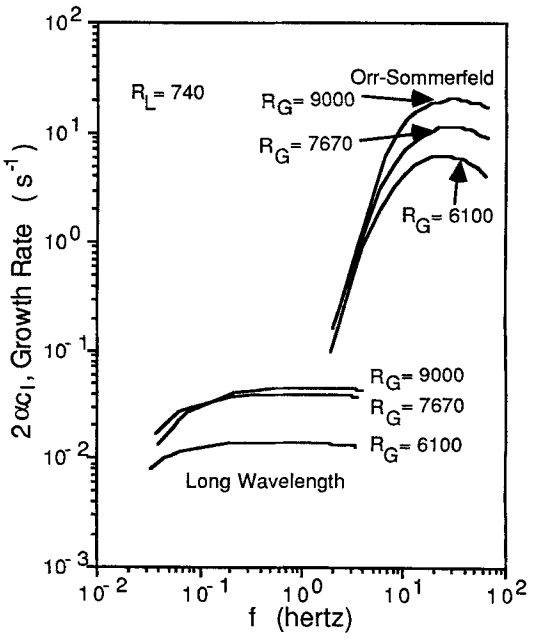

Figure 5. Plot of growth rate as a function of gas Reynolds number for two wave types.

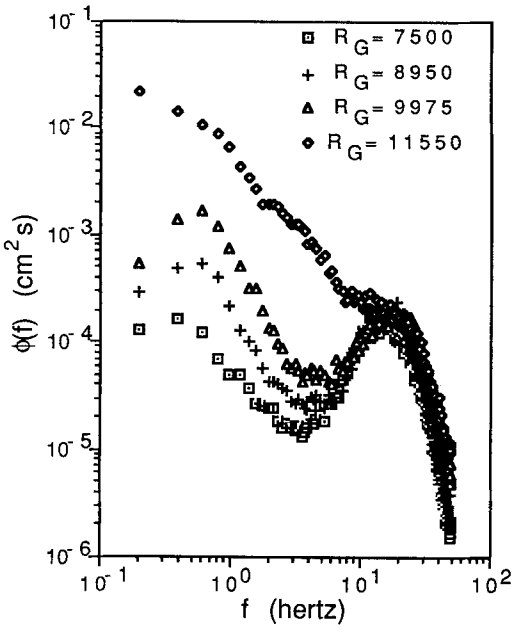

Figure 6. Measured wave spectra as a function of gas Reynolds number across the visual roll wave transition.

Roll waves are present only for the highest gas Reynolds number.

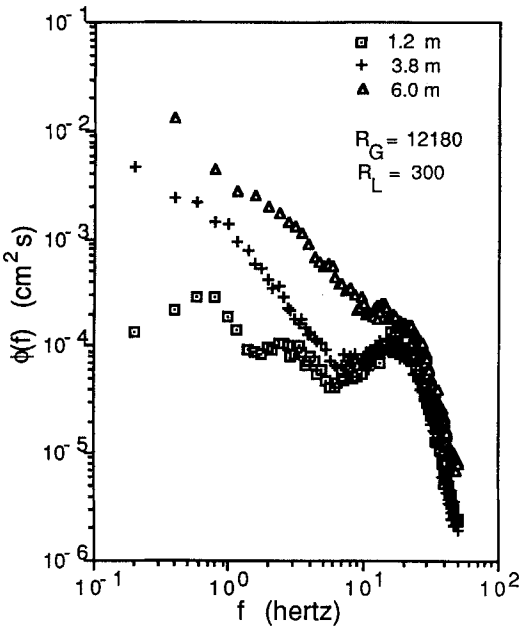

Figure 8. Wave spectra as a function of fetch at a gas Reynolds number above the roll wave transition.

peak occurs. In Figure 8, similar measurements are taken at a gas Reynolds number just above the roll wave transition. Identical qualitative behavior is observed with roll waves becoming visible near the end of the channel when the wave slope becomes large enough for the wave to break.

Waves were induced artificially by a paddle oscillating at 0.8 Hz at a R_G below the roll wave transition. The resulting spectral measurements with and without paddling are shown in Figure 9. Again the qualitative behavior is the same but roll waves were observed near the end of the channel for the case where waves were artificially induced. The paddle created small amplitude waves which were initially large enough so that with continual growth, they began to break before the end of the channel. These data provide further support to the idea that roll waves are the end result of continuous slow growth of low-frequency waves. The transition must consequently be a function of fetch, and for long channels it is expected that roll waves would appear at R_G lower than the observations reported by Andreussi et al. (1985) or our current observations.

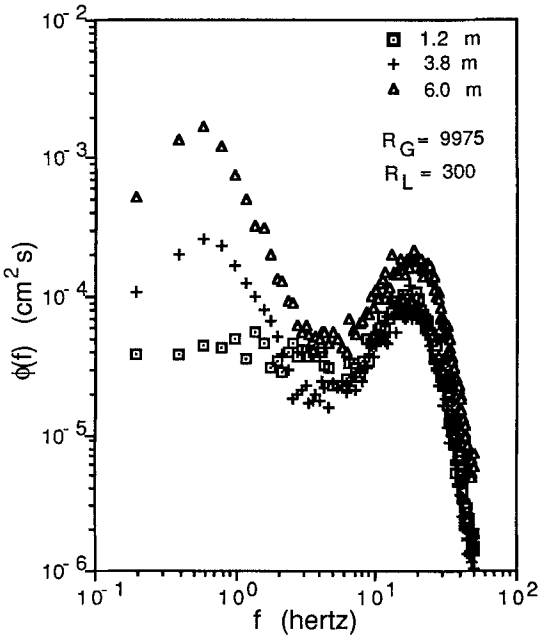

Figure 7. Wave spectra as a function of fetch at a gas Reynolds number below the roll wave transition.

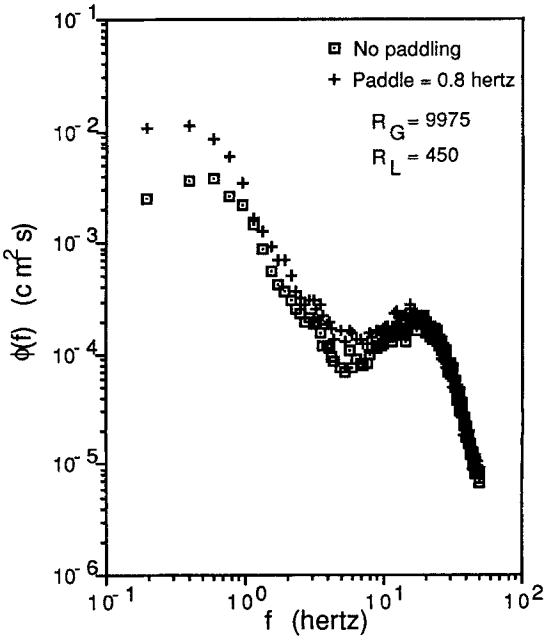

Figure 9. Wave spectrum at large fetch with paddle-induced waves.

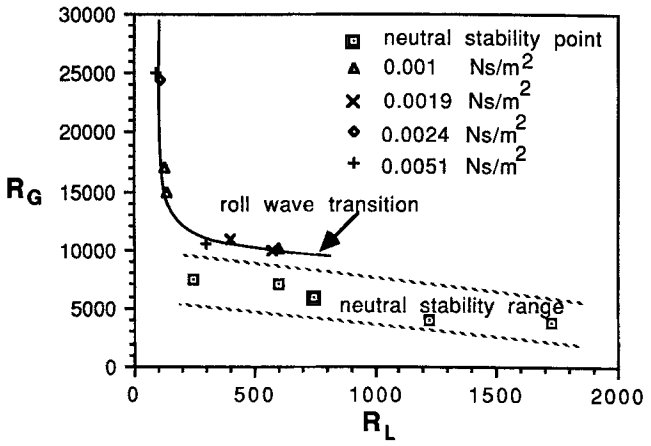

Figure 10. Visual roll wave transition and prediction of the location of neutral stability of long-wavelength waves.

Results of the long-wavelength stability analysis are shown in Figure 10 with the squares indicating our predictions for the location of neutral stability obtained from calculations based on our experimental data. Long waves are predicted to be unstable at gas Reynolds numbers above the locations of the symbols. We note that as the change of the growth rate occurs slowly over a large R_G range, Figure 5, and that all of the parameters are not known with great accuracy, the predicted transition should be viewed as occurring within the region bounded by the dashed lines, which depict our estimate of the total error in the calculation, rather than on a single curve. The data shown in Figure 6, for which long waves are observed at all measured R_G, agree with the predictions. Below a R_G of about 6,000, spectra which we have examined show no evidence of long-wavelength disturbances again in agreement with the predicted transition.

Also shown on Figure 10 is the complete roll wave transition curve reported by Andreussi et al. (1985) and some of our observations. The transition is seen to exhibit two different types of behavior. For R_L less than about 150, the transition changes from depending on R_G to depending rather dramatically on R_L. For water, the transition occurs at $R_L \sim 100$ for all R_G. In this region, the data of Andreussi et al. (1985) indicate that, as the liquid viscosity increases, roll waves occur at a somewhat lower R_L.

It is of interest to perform experiments similar to those presented above to examine the roll wave transition for low R_L. Figure 11 shows the wave spectrum measured at increasing R_L across the roll wave transition. A rather sudden change in the spectrum occurs when roll waves appear. The low-frequency region, which without roll waves has relatively little energy, increases by over an order of magnitude with a small increase in R_L. The data at lower R_L do not indicate the presence of any low-frequency waves which may be precursors of roll waves. In Figure 12, the spectrum as a function of fetch is given for conditions where no roll wave transition occurs showing very little change. However, Figure 13 shows that for R_L above 100, a secondary wave peak appears and grows rapidly with increasing distance in a fashion almost identical to the thick film case shown in Figure 8.

Discussion

$R_L > 200$

The data presented in Figures 3, 5, 6, 7, 8 and 9 provide convincing evidence that roll waves form from low-frequency disturbances as has been suggested previously by Hanratty and Hershman (1961) and Andreussi et al. (1985). However, just as clear is the observation that these long-wavelength disturbances can exist for long periods of time (or distance) before growing

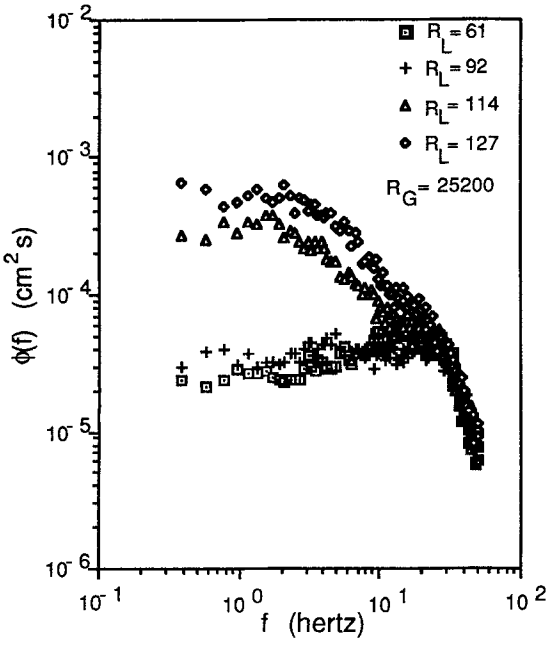

Figure 11. Measured wave spectra as a function of liquid Reynolds number across the visual roll wave transition.

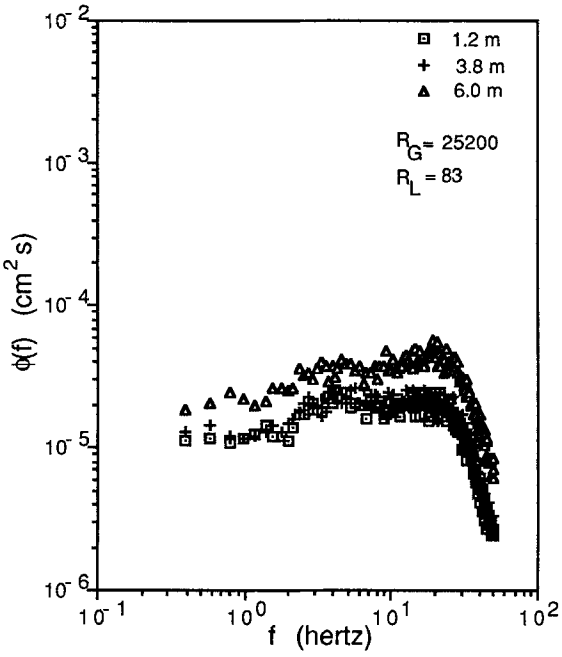

Figure 12. Measured wave spectra as a function of fetch at a liquid Reynolds number below the roll wave transition.

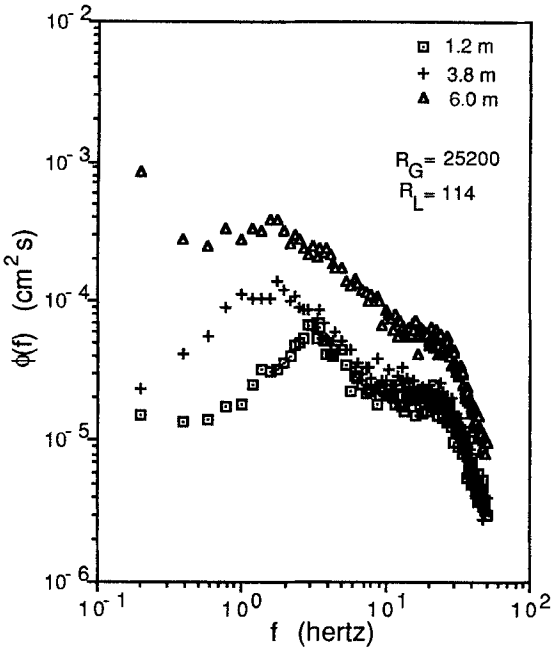

Figure 13. Wave spectra as a function of fetch at a liquid Reynolds number above the roll wave transition.

large enough to break. As a consequence, while the idea of using linear stability theory to predict slowly forming phenomena such as roll waves is reasonable, the issue of the length of time (or distance) required for formation must also be addressed. It is clear from the measurements that, depending on the gas Reynolds number, roll waves may take on the order of 5–10 s to appear in our flow system. Therefore, when observations of transitions of slowly growing disturbances are involved, they should be reported as a function of fetch.

A related issue is the procedure for determining the neutral stability conditions. In our calculation, the complete Eigenvalue problem was solved yielding predictions of growth rates. This would seem to be a safer procedure than simply finding conditions where the growth rate was zero as it clearly demonstrates the sensitivity of growth rate on flow parameters as well as how errors in the knowledge of these parameters affect the predicted stability boundaries. The error bounds shown on Figure 10 indicate our estimates for the location of neutral stability given the effects of all of the uncertainties in the various parameters.

In an attempt to reproduce the neutral stability results of Hanratty and Hershman (1961) and Andreussi et al. (1985) which agree with the visually observed roll wave transition, we found that the variation of $\overline{\Gamma}$ with Reynolds number appeared to be the reason that our predictions disagree with previous work. As mentioned above, they relied on the self-similarity of the profiles. Our determination of the velocity profile, by fitting it to the measured average flow variables (interfacial stress, film height, etc.), suggests that the profiles are not self-similar and as a consequence, our prediction of the location of neutral stability should be more reliable. Furthermore, our prediction of instability agrees closely with appearance of a low-frequency peak in the wave spectra which occurs at gas Reynolds numbers well below the visual roll wave transition.

An issue which cannot be resolved by any linear theory is whether the long waves, once unstable, must always eventually grow until they break or if factors occur which can stabilize them. None of our measurements indicate that stable long-wavelength waves exist, in every case continual growth with fetch was observed. Nonlinear analyses of the Dressler equation, which has similar qualitative properties to Eq. 2, by Needham and Merkin (1984) indicate that stable waves of finite form are found mathematically if a term accounting for the presence of shear stresses normal to the flow were included. A coefficient of eddy viscosity is needed to describe the magnitude of these stresses. As the viscosity coefficient is taken as an adjustable constant, we are somewhat skeptical that this mode of stabilization is likely to occur for our flows. Other possible modes of stabilization are interactions with small wavelength waves and direct the effect of surface tension which may become important when regions of high curvature form just prior to breaking. Resolution of this issue will require a complete nonlinear analysis of the flow.

$R_L < 200$

For thinner films, the data and theory do not provide a conclusive explanation for the origin of roll waves. The spectral data indicate that for R_L below ~100, a low frequency wave peak is not observed even at very high gas velocities; but as R_L is increased, roll waves suddenly appear. An extension of our linear stability analyses to smaller R_L would show only a slight increase in the value of the gas Reynolds number at neutral stability (Hanratty and Hershman, 1961), and examination of Eq. 10 does not reveal any sensitivity of the growth rate to small changes in R_L. Andreussi et al. (1985) suggest that, for values of R_L less than the observed transition, the phase angle of the interfacial stress is such that the shear stress variation could be responsible for delaying instability. They claim that near the value of R_L where the transition is observed, a large change in the phase angle of the stress occurs because of a sudden roughening of the liquid surface. As can be seen in figure 11, no large change in the high-frequency wave peak which could be associated with an increase in surface roughness occurs. As a consequence, it seems that such a large change in the phase lag is unlikely to occur with a small increase in the liquid Reynolds number. However, if such a phase shift did occur, the qualitative behavior of the low-frequency part of our spectra would be explained well by the linear instability of a long-wave disturbance occurring with a small increase in liquid Reynolds number.

Another possible explanation, which is consistent with previous nonlinear wave studies and our experiments can be given. Our observations indicate that, for liquid viscosities greater than about 1.0×10^{-2} N · m/s^2, no actual breaking was occurring. For these higher liquid viscosities, the roll wave transition shown in Figure 3 of Andreussi et al. (1985) appears to be associated with transition from a periodic type of wave behavior to a solitary type of wave behavior. The waves change in form from nearly sinuous to more of a triangular shape with a steep front and a shallow back. This leads us to suggest that, for thin films with high viscosities, "roll waves" are actually solitary waves which have begun to break. Since the transition in figure 3 of Andreussi et al. (1985) is seen to be a monotonic function of viscosity, it may be that qualitatively similar behavior occurs at all viscosities. Consequently, thin-film roll waves may not be the

result of a linear instability but actually the final wave form which occurs in the evolution of finite amplitude waves.

Conclusions

Data and calculations presented above support the contention by Hanratty and Hershman (1961) and Andreussi et al. (1985) that roll waves form from slowly growing disturbances which have wavelengths much longer than the film thickness. However, because the long-wavelength disturbances from which the roll waves originate are shown to be unstable at gas Reynolds numbers much lower than previously thought, the absolute criteria for transition which they have presented appear to be incorrect. Precursor waves are growing slowly with fetch and it is expected that for long conduits, roll waves will appear at R_G below the values predicted by Andreussi et al. (1985). For thinner films, the data do not give conclusive proof for the origin of roll waves but it is speculated that these are actually solitary waves which have begun to break. As a consequence, nonlinear analyses, such as was done by Chang (1987) for waves on falling films, are needed to describe their behavior.

Acknowledgment

The Authors would like to thank the donors of the Petroleum Research Fund, administered by the American Chemical Society, and the Engineering Foundation through grant RI-A-85-14 for partial support of this research.

Notation

a = wave amplitude, real number
$A(R_L)$ = function used to define wall shear stress
A_T, B_T, C_T, D_T = turbulent velocity profile coefficients
B = height of gas space above the average film height
c = complex wave velocity
f = frequency, Hz
f_s = gas-liquid flow friction factor
g = acceleration of gravity
h = instantaneous film height
h_g^+ = correlated function of R_L
h^+ = $(hv)^*/\nu$, dimensionless
n = dimensionless exponent
p = liquid phase pressure
P = gas phase pressure
R_L = liquid Reynolds number
R_G = gas Reynolds number
t = time
u = x-direction liquid velocity
u^+ = u/v^*
U = x-direction gas velocity
v = y-direction liquid velocity
v^* = friction velocity
$\overline{u'v'}$ = turbulent stress term
x = flow direction coordinate
y = coordinate perpendicular to x

Greek letters

α = radian wave number
ϕ = universal spectral function
Γ = velocity profile shape factor
μ = molecular viscosity
ν = kinematic viscosity
ρ = density
σ = surface tension
τ = shear stress

Superscripts

$'$ = fluctuating quantity
$\hat{}$ = $a\hat{\zeta}$ is a complex amplitude of fluctuating quantity ζ
$\bar{}$ = time averaged quantity

Subscripts

a = average over y
B = upper wall
G = gas
I = imaginary part of a complex number
L = liquid
s = gas-liquid interface
R = real part of a complex number
T = denotes a constant in the turbulent velocity profile
w = bottom wall

Literature Cited

Abrams, J., "Turbulent Flow over Small Amplitude Solid Waves," PhD Thesis, Univ. of Illinois, Urbana (1984).

Andreussi, P., J. C. Asali, and T. J. Hanratty, "Initiation of Roll Waves in Gas-Liquid Flows," *AIChE J.*, **31,** 119 (1985).

Chang, H.-C., "Evolution of Nonlinear Waves on Vertically Falling Films—A Normal Form Analysis," *Chem. Eng. Sci.*, **42,** 515 (1987).

Chu, K. J., and A. E. Dukler, "Statistical Characteristics of Thin, Wavy Films: II. Studies of the Substrate and its Wave Structure," *AIChE J.*, **20,** 695 (1974).

———, "Statistical Characteristics of Thin, Wavy Films: III," *AIChE J.*, **21,** 583 (1975).

Cohen, L. S., and T. J. Hanratty, "Generation of Waves in the Concurrent Flow of Air and a Liquid," *AIChE J.*, **11,** 138 (1965).

Craik, A. D. D., "Wind-Generated Waves in Thin Liquid Films," *J. Fluid Mech.*, **26,** 369 (1966).

Dukler, A. E., "Role of Waves in Two Phase Flow: Some New Understandings," *Chem Eng. Ed.*, **11,** 108 (1977).

Hanratty, T. J., and J. M. Engen, "Interaction between a Turbulent Air Stream and a Moving Water Surface," *AIChE J.*, **3,** 299 (1957).

Hanratty, T. J., and A. Hershman, "Initiation of Roll Waves" *AIChE J.*, **7,** 488 (1961).

Hanratty, T. J., "Interfacial Instabilities Caused by Air Flow," *Waves on Fluid Interfaces,* Academic Press, ed., R. E. Meyer, 221 (1983).

Henstock, W. H., "The Effect of a Cocurrent Gas-Flow on Gas-Liquid Mass Transfer," PhD Thesis, Univ. Of Illinois, Urbana (1977).

Henstock, W. H., and T. J. Hanratty, "The Interfacial Drag and the Height of the Wall Layer in Annular Flows," *AIChE J.*, **22,** 990 (1976).

Jeffreys, H., "On the Formation of Water Waves by Wind," *Proc. Roy. Soc. Lond.*, **A107,** 189 (1925).

Kordyban, E., "Some Details of Developing Slugs in Horizontal Two-Phase Flow," *AIChE J.*, **31,** 802 (1985).

Lin, P. Y., "Flow Regime Transitions in Horizontal Gas-Liquid Flows," PhD Thesis, Univ. of Illinois, Urbana (1985).

Martin, C. J., and B. J. Azzopardi, "Waves in Vertical Annular Flow," *Physicochem. Hydrody.*, **6,** 257 (1985).

McCready, M. J., "Spectral Behavior of Capillary Waves in Gas-Liquid Flows," *Phys. of Fluids,* **29,** 2836 (1986).

Miya, M., "Effect of Waves on Turbulence," MS Thesis, Univ. of Illinois, Urbana (1968).

Miya, M., D. E. Woodmansee, and T. J. Hanratty, "A Model for Roll Waves in Gas-Liquid Flows," *Chem. Eng. Sci.*, **26,** 1915 (1971).

Needham, D. J., and J. H. Merkin, "On Roll Waves Down an Open Inclined Channel," *Proc. Roy. Soc. Lond., Ser. A.*, **394,** 259 (1984).

Nencini, F., and P. Andreussi, "Studies of the Behavior of Disturbance Waves in Annular Two-Phase Flow," *Can. J. Chem. Eng.*, **60,** 459 (1982).

Pai, S. I., "On Turbulent Flow between Parallel Plates," *J. App. Mech.*, **20,** 109 (1953).

Telles, A. S., and A. E. Dukler, "Statistical Characteristics of Thin, Vertical, Wavy, Liquid Films," *Ind. Eng. Chem. Fund.*, **9,** 412 (1970).

Webb, D. R., and G. F. Hewitt, "Downwards Cocurrent Annular Flow," *Int. J. Multiphase Flow,* **2,** 35 (1975).

Woodmansee, D. E., and T. J. Hanratty, "Mechanism for the Removal of Droplets from a Liquid Surface by a Parallel Air Flow," *Chem. Eng. Sci.*, **24,** 299 (1969).

Manuscript received Feb. 22, 1988, and revision received May 6, 1988.